PHYSICAL REVIEW B **90**, 205212 (2014)

Towards understanding the hydrogen molecule in ZnO

S. G. Koch,* E. V. Lavrov,† and J. Weber
Technische Universität Dresden, D-01062 Dresden, Germany
(Received 18 September 2014; published 17 November 2014)

The hydrogen molecule H_2 (or "hidden" hydrogen) in ZnO is studied by Raman scattering spectroscopy. It is shown that H_2 is practically a free rotator stable up to 700 °C, which is formed by two mobile interstitial hydrogen atoms. The concentration profile of the hydrogen molecule anticorrelates with hydrogen substituting for oxygen (H_O) created at the sample surface during the high temperature hydrogenation. The H_2 dissociation at elevated temperatures in the bulk regenerates interstitial (H_{BC}) hydrogen, whereas the formation of H_O and hydrogen out-diffusion are dominant decay channels of the molecule near the surface. The latter mechanisms are responsible for the lower stability of H_2 in the subsurface region. An ortho-para conversion between the nuclear spin states 1 and 0 of the molecule at 79 K was found to occur within 7.5 h, whereas the back conversion at room temperature occurs faster than 0.5 h. A shift in frequency of the H_2 local vibrational mode with annealing time and temperature is associated with the thermal anneal of lattice imperfections. The coupling of transitions between rotational states of the molecule and lattice phonons influences the ro-vibrational properties. Interstitial lattice sites and/or larger vacancy clusters are preferred trapping centers for H_2 in ZnO.

DOI: 10.1103/PhysRevB.90.205212 PACS number(s): 61.72.J−, 63.20.Pw, 67.63.Cd, 78.30.Fs

I. INTRODUCTION

Molecular hydrogen (H_2) in semiconductors was theoretically predicted to be stable already in the 1980s [1,2]. Since then, experimental evidences for the H_2 presence were found in GaAs [3], Si [4,5], and Ge [6] where the molecule can be trapped at various lattice sites.

The existence of H_2 in ZnO was originally proposed by Shi *et al.* who argued that some hydrogen in the crystal may exist in the "hidden" form, i.e., be electrically neutral and invisible for IR absorption [7]. Raman scattering studies established molecular hydrogen via detection of local vibrational modes (LVMs) of H_2 and its isotopes [8].

H_2 exhibits two total nuclear spin states $I = 0$ (para state, p-H_2) or 1 (ortho state, o-H_2). The fermionic nature of hydrogen nuclei limits the corresponding rotational quantum number J to an even or odd value, respectively [9]. In free space the transition time between both species is huge, exceeding the lifetime of the universe [10]. Because of this, the natural abundance ratio of the two species (o:p) is determined by the nuclear spin degeneracy and in the absence of external perturbation remains constant at 3:1. In Raman scattering the ortho-to-para ratio is directly reflected by the vibrational transitions $Q(0)$ and $Q(1)$ at 4161 and 4155 cm^{-1}, respectively [11].

Rotational and vibrational states of H_2 are affected if the molecule is placed in a semiconductor host. Experimentally, a decrease of the LVM frequency is observed. This finding is explained by the weakening of the hydrogen bond due to the screening by the electron density from the surrounding host atoms [12]. In Si, the interaction with the host and/or trapping centers also results in an ortho-to-para conversion of H_2, which was found to strongly depend on the nature of the defect complexes [13–17]. So far, an unambiguous mechanism explaining the nuclear spin flip of H_2 in Si has not been proposed [13,15]. For other semiconductors ortho-para conversion between o- and p-H_2 has not been reported.

First principles calculations suggest that hydrogen molecules in ZnO are stable and located at an interstitial lattice site [18,19]. The conclusions of the theory are supported by the results of the Raman scattering studies which revealed that the LVM of H_2 at 4145 cm^{-1} is split into two components separated by 8 cm^{-1} with an intensity ratio of approximately 3:1 assigned to o- and p-H_2 [8]. Theoretical considerations by Karazhanov and Ulyashin, however, suggest H_2^* as the ground state of the hydrogen dimer in unstrained ZnO. The complex comprises two weakly coupled hydrogen atoms each of which is bound to the neighboring oxygen and zinc atoms [20]. In the case of strained and oxygen-deficient ZnO the configuration of separated hydrogen substituting for oxygen (H_O) and interstitial hydrogen (H_{BC}) was found to be more stable than H_2^* [21]. Contrary to these authors, Du and Biswas claim that molecular hydrogen in ZnO is stable but located within the oxygen vacancy rather than at an interstitial lattice site [22]. Experimentally, the issues related to the formation, stability, and position in the lattice of hydrogen dimers in ZnO have not been addressed yet.

Here, we present the results of a Raman scattering study of molecular hydrogen in ZnO. We discuss the formation process, the thermal stability, the interplay with the lattice phonons, the interaction with other hydrogen-related defects, the position in the host lattice, as well as the ortho-para conversion rates.

II. EXPERIMENTAL

The ZnO samples used in this study were nominally undoped vapor phase grown single crystals grown at the Institute for Applied Physics, University of Erlangen (Germany) [23,24]. Hydrogen was incorporated at temperatures of 800–1000 °C for 1 h with the samples placed in sealed quartz ampoules filled with H_2 gas (pressure of 0.5 bar at room temperature). This thermal treatment was terminated by quenching the sample to room temperature in water. For

*sandro.koch@physik.tu-dresden.de
†Also at Institute of Radioengineering and Electronics, Mokhovaya 11, 101999 Moscow, Russia.

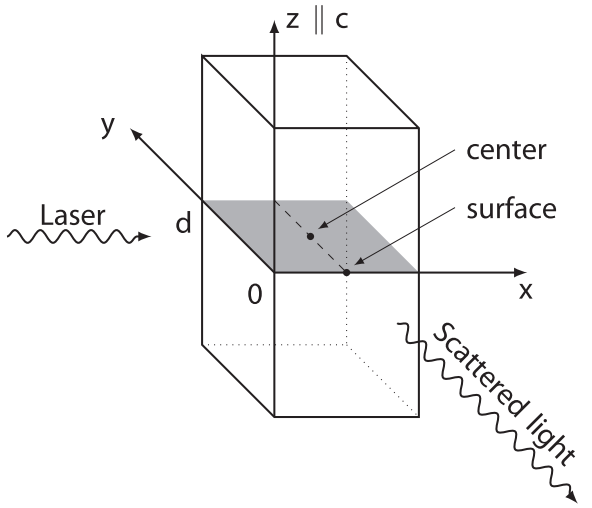

FIG. 1. Sketch of the Raman scattering geometry employed in this study. Depth profile measurements were performed along the dashed line. The scattering position in the middle of the sample and at the surface are labeled "center" and "surface," respectively. The sample thickness is denoted by "d."

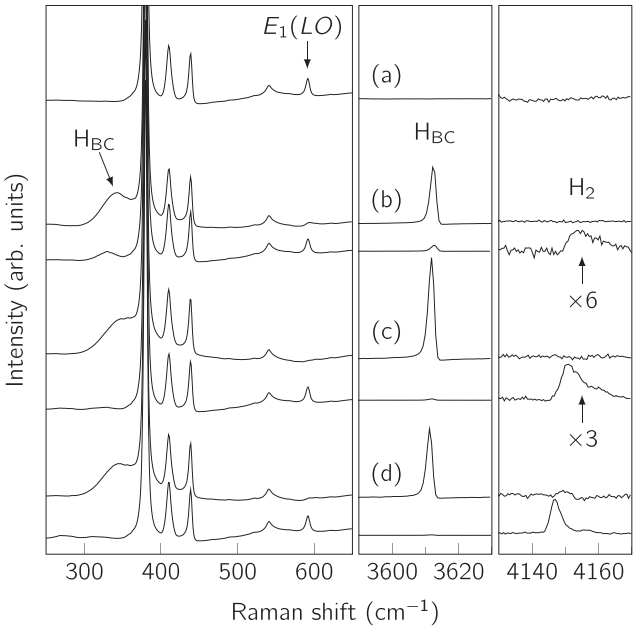

FIG. 2. Raman spectra obtained at $T \leqslant 55$ K for an as grown (a) and hydrogenated ZnO crystals with the hydrogenation temperatures of 800 °C (b), 900 °C (c), and 1000 °C (d). The upper curves refer to the as treated samples, whereas the lower ones were obtained after annealing in Ar at 500 °C.

isotope substitution experiments, hydrogen was replaced either by deuterium or by a mixture of H_2 and D_2 (1:1). Directly after hydrogenation the samples exhibited a gray surface which was removed via polishing of about 50–150 μm from each face of the sample. Subsequent annealing steps were carried out in Ar atmosphere for 0.5–1 h in the temperature range 100–1000 °C.

The Raman measurements were performed in 90° geometry using the frequency doubled 532-nm line of a Nd:YVO_4 laser with a power of 1 W for excitation in the temperature range 50–300 K. The scattered light was analyzed using a single grating monochromator and a liquid-nitrogen-cooled Si CCD detector array. The spectral resolution was 2.5–3.6 cm^{-1}. The integration time depended on the spectral region and ranged from 1 min for the phonon spectrum of ZnO to 2 h for the hydrogen-related vibrational modes. To account for misalignments in the sample mounting, Raman spectra were calibrated with respect to the intensity and frequency of the A_1(TO) phonon mode at 380 cm^{-1}.

The scattering geometry is defined in the coordinate system of the sample, with the x, y, and z axes parallel to the $[10\bar{1}0]$, $[1\bar{2}10]$, and c axes, respectively. If not noted otherwise the $x(z-)y$ configuration was employed [25]. Here "–" indicates that no polarization for the scattered light was selected. The laser was focused on the dashed line shown in Fig. 1. At this position the laser beam exhibits a minimal diameter of about 35 μm.

Laser light scattered only from points on the dashed line was selected by using a mask placed on the xz face of the sample. Depth profiles were obtained via shifting the sample along the y direction and recording the spectra as a function of y.

III. RESULTS

A. Formation process

In order to investigate the formation process of H_2, a ZnO sample was hydrogenated at 800 °C and subsequently annealed at 500 °C for 1 h in Ar. This procedure was repeated with the same sample for the hydrogenation temperatures of 900 and 1000 °C. Raman spectra of this sample recorded with the excitation laser focused in the center of the sample are presented in Fig. 2. The hydrogenation results in the formation of bond-centered hydrogen (H_{BC}), which reveals the $1s \rightarrow 2s(2p)$ shallow donor transition at ~330 cm^{-1} and the LVM at 3611 cm^{-1} as well as the quenching of the E_1(LO) phonon line due to the Fano resonance with the energy spectrum of the electronic states in the conduction band [26].

Subsequent annealing at 500 °C eliminates the H_{BC}-related signals and recovers the E_1(LO) phonon line, since the concentration of shallow donors is significantly reduced. The $1s \rightarrow 2s(2p)$ transition of another hydrogen-related shallow donor H_O at around 265 cm^{-1} is too weak to be detected in our spectra, because the amount of oxygen vacancies in the bulk of the sample is marginal compared to that at the sample surface [27].

The annealing also results in the appearance of a broad band close to the LVMs of H_2. With increasing hydrogenation temperature the peak intensity of this signal grows in, the line narrows, and the frequency decreases approaching the value reported previously for H_2 in ZnO [8].

This result agrees with an earlier suggestion that the molecule is formed via trapping of two mobile H_{BC} [26]:

$$H_{BC}^{+} + H_{BC}^{+} + 2e^{-} \rightleftharpoons H_2. \quad (1)$$

The red-shift of the LVM frequencies due to the molecule with increasing hydrogenation temperature [see Figs. 2(b)–2(d)] indicates a significant dependence of the amount of lattice damage on the temperatures of the two-step "hydrogenation-annealing" treatment as will be discussed below in more detail.

The overall intensity of the H_{BC}-related signals in the sample hydrogenated at 1000 °C is somewhat less compared to that treated at 900 °C. On the other hand, the solubility limit of hydrogen quadruples as the temperature enhances from 800 °C to 1000 °C [28]. This is in good agreement with the intensity ratio 4.6 ± 0.8 of the H_2-related signals in Figs. 2(b) and 2(d). We take this as an indication that the high temperature treatment creates additional traps for hydrogen, e.g., zinc and/or oxygen vacancy agglomerates, which decreases the amount of interstitial hydrogen [27]. Annealing at 500 °C releases hydrogen from these traps, thus enhancing the concentration of H_2.

The coupling of the E_1(LO) phonon and the plasmon vibrations mediated by the Coulomb interaction leads to a frequency shift and line broadening of the E_1(LO)-like phonon-plasmon proportional to the free carrier concentration [29,30]. After hydrogenation of the sample at 800 °C the E_1(LO) mode observed at room temperature strongly broadens. The observed blue-shift of $12 \pm 4\ \mathrm{cm}^{-1}$ corresponds to a free carrier concentration of $(3.4 \pm 1.1) \times 10^{17}\ \mathrm{cm}^{-3}$. Since the line shape is additionally affected by the Fano resonance, this value is only a rough estimation. At elevated hydrogenation temperatures the line intensity drops below the detection limit of our setup preventing us from a direct verification of the correlation between the free carriers and the LVM intensity of H_{BC}. Previously, however, we have established that the H_{BC} concentration after hydrogenation at 1000 °C is about $5 \times 10^{17}\ \mathrm{cm}^{-3}$ [27]. From the comparison of the LVM intensities in Fig. 2 the H_{BC} concentration after the 800 °C treatment is about $4.2 \times 10^{17}\ \mathrm{cm}^{-3}$. This value agrees well with the free carrier concentration and gives further evidence that H_{BC} is the predominant shallow donor directly after the treatment. After annealing in Ar the majority of H_{BC} in the bulk is converted into H_2 (see below) indicating an H_2 concentration of the same order of magnitude.

B. Thermal stability

1. Isochronal annealing

Figure 3 presents Raman spectra of an isochronal annealing series of ZnO samples which were treated in H_2, D_2, and a mixture of D_2 and H_2 at 1000 °C. Spectra on the top of the

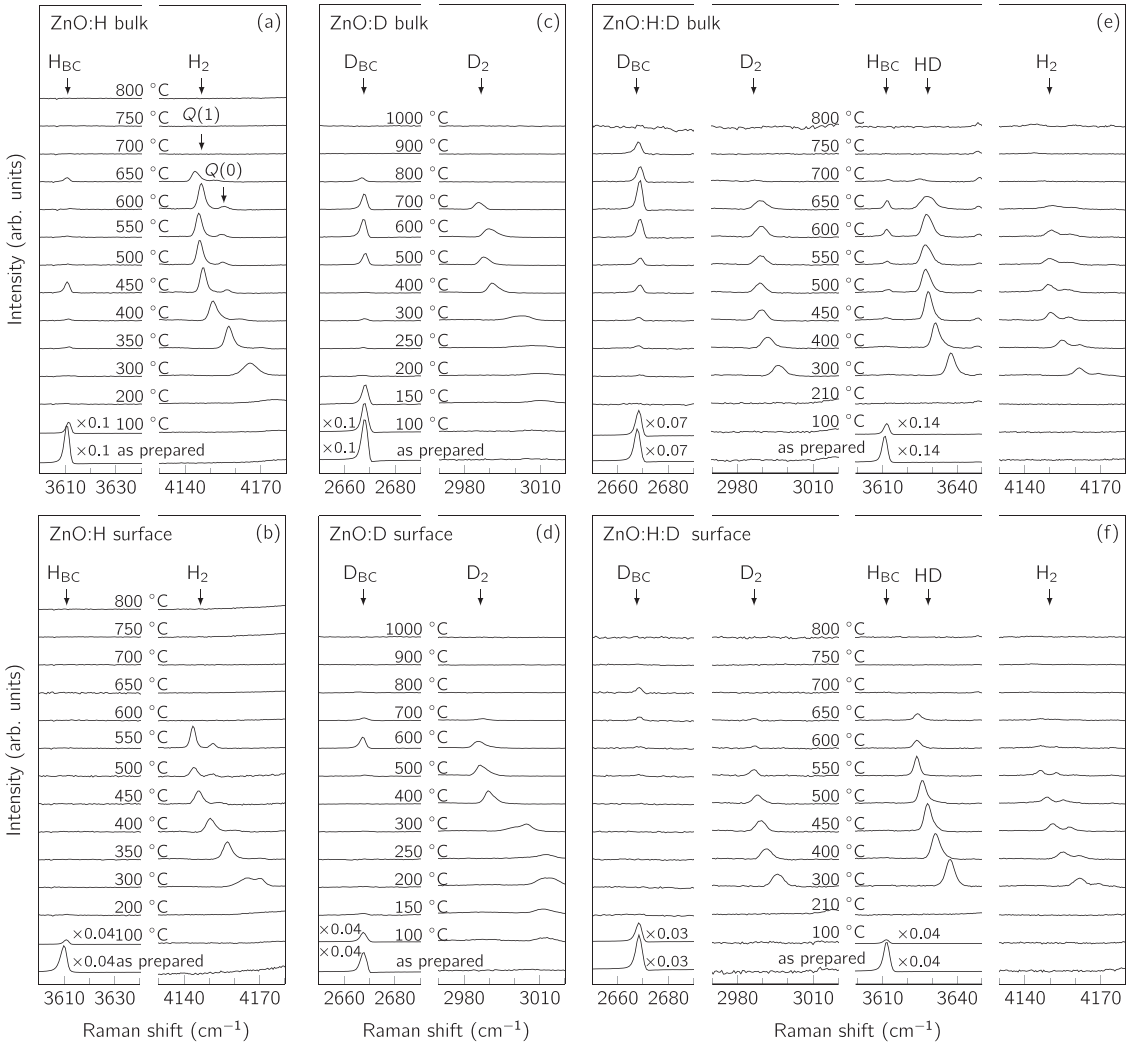

FIG. 3. Isochronal annealing series of a hydrogenated (left), deuterated (middle), and hydrogenated and deuterated (right) ZnO sample. The Raman spectra were recorded from the bulk (top) and near the sample surface (bottom) at $T \leqslant 55$ K. The spectra at some temperatures are scaled by the depicted factor.

figure were recorded with the laser focused in the center of the sample, whereas those on the bottom were taken with the scattering volume close to the sample surface.

The behavior of the hydrogen-related defects, e.g., H_{BC} and H_O, for annealing temperatures below 200 °C is discussed elsewhere (see Ref. [27]). No LVMs due to the hydrogen molecule are detected for these annealing temperatures.

After annealing of ZnO:H at 200 °C a weak and broad feature at 4175 cm^{-1} appears in the bulk of the sample [see Fig. 3(a)]. This signal experiences a significant narrowing and red-shifts by 8 cm^{-1} after annealing at 300 °C. Note, that these values are above the frequency of free H_2 at 4161 cm^{-1} [11]. The formation of hydrogen molecules at 300 °C agrees with earlier IR absorptions investigations [7] and with recent Hall measurements on ZnO:Al and $Zn_{1-x}Mg_xO$:Al films [31]. The appearance of H_2 directly after the quenching of H_{BC} gives further support of reaction (1). With increasing temperature, the band red-shifts and narrows until its frequency approaches 4145 cm^{-1} and reveals the two components due to *o*- and *p*-H_2 [8]. At 650 °C the molecule starts to dissociate with H_{BC} being the end-products. After annealing the sample at 700 °C no H_2 can be seen in the spectra.

Figure 3(b) shows the results of an identical annealing series conducted at the surface of the same sample. The behavior of H_2 is basically similar to that in the bulk except that the signal disappears already at 600 °C. On the other hand, no spectroscopic features of H_{BC} were detected for the annealing temperatures above 200 °C. Instead, the hydrogen is trapped by the oxygen vacancies generated at the sample surface by high temperature treatment resulting in the formation of the H_O shallow donor [27].

The results of a similar measurement series obtained for the ZnO:D sample are presented in Figs. 3(c) and 3(d). Isotopic substitution of hydrogen with deuterium practically does not change the frequencies of the electronic transitions, whereas LVMs red-shift by a factor of about $1/\sqrt{2}$. With respect to the thermal stability, deuterium-related defects anneal out at higher temperatures as compared to hydrogen. We explain this finding by the smaller mobility of deuterium compared to hydrogen resulting from its heavier mass and smaller zero-point energy [26].

Finally, the results obtained for the ZnO:H:D sample are presented in Figs. 3(e) and 3(f). In addition to the lines discussed above, a local vibrational mode of the HD molecule appears at 3637 cm^{-1} after annealing the sample at 210 °C. The line position stabilizes at 3628 cm^{-1} for annealing temperatures exceeding 500 °C.

The final LVM frequencies of the molecules match the values that have been reported previously [8]. Note that the limited resolution of our setup did not allow us to observe the ortho-para splitting of D_2.

Hydrogen molecules located at the sample surface anneal out at lower temperatures compared to those in the bulk. We explain this behavior as follows. At elevated temperatures H_2 partially dissociates into the H_{BC} species which diffuse towards the surface of the sample. The reappearance of the H_{BC} (D_{BC}) signal already after annealing at 450 °C in the bulk supports our suggestion. A reappearance of the bond-centered hydrogen was reported previously for low temperature hydrogenated ZnO by Shi *et al.* [32]. A similar behavior was observed after annealing ZnO samples at 400 °C for the zinc vacancy decorated with two hydrogen atoms and a hydrogen-related mode at 3326 cm^{-1} [7,33,34]. At the surface, however, interstitial hydrogen either outdiffuses or gets trapped by the subsurface oxygen vacancies thus accounting for the missing H_{BC} in the Raman spectra [27].

Interestingly, the isochronal annealing series also show that not only the intensities of the Raman lines due to the molecular hydrogen but also the frequencies of the corresponding LVM modes depend on the annealing temperature. We take this as an indication that the apparent properties of the molecule are affected by some other, not yet identified defect(s) introduced into ZnO samples via the process of high temperature hydrogenation.

In order to get insight into the effect of the annealing temperature on the lattice potential, we consider the LVM frequency shift in more detail. Molecular vibrations can be well described by the Morse potential [35],

$$V(r) = D_0[\exp(-2\alpha[r - r_0]) - 2\exp(-\alpha[r - r_0])], \quad (2)$$

where D_0 is the dissociation energy, α defines the anharmonicity and potential width, whereas r_0 is the equilibrium distance between the hydrogen nuclei. The eigenvalues of the rotational-vibrational Hamiltonian are given by [9]

$$E(\nu, J) = \hbar\omega_e\left(\nu + \tfrac{1}{2}\right) - \chi_e\hbar\omega_e\left(\nu + \tfrac{1}{2}\right)^2 + E_{\mathrm{ro}}(J) + E_{\mathrm{rovib}}(\nu, J), \quad (3)$$

where ω_e is the harmonic frequency and χ_e stands for the anharmonicity. A detailed analysis of the relation between the Morse potential parameters and the $Q(J)$ mode frequencies can be found in the literature [35,36].

The ortho-para splitting Δ_{op} caused by the ro-vibrational coupling depends on the interatomic distance in the molecule. *Ab initio* calculations revealed a linear relation between the force constant k and the interatomic distance r_0 in semiconductors [12]. From the experimental values of gaseous H_2 and interstitial H_2 in Si as well as the relation $k = \mu\omega_e^2$ we determine

$$r_0(\text{Å}) = -0.007548\,k\ (\text{eV/Å}^2) + 1.013531. \quad (4)$$

The results for the different annealing steps of the deuterated/hydrogenated ZnO sample are summarized in Table I. Some values known from the literature for other hosts are listed below for comparison [11,37–39].

With increasing annealing temperature the dissociation energy D_0 slightly decreases, whereas the parameter α marginally increases. The interatomic distance remains almost constant during the annealing procedure. This finding indicates that the frequency shift is mainly caused by a change of the dissociation energy. All values, except χ_e, are in reasonable agreement with that of gaseous H_2 and H_2 trapped in Si platelets, which supports the model of a free rotating molecule and indicates that the Morse potential can explain the vibrational properties of H_2 in ZnO reasonably well. The anharmonicity parameter χ_e deviates from that of the gaseous species by about 5%–8%, which results in the blue-shift of the $Q(J)$ modes above 4161 cm^{-1}. The calculated ortho-para splitting differs from the experimental observation by a factor of 1.7–2.

TABLE I. Ro-vibrational properties and lattice potential of H_2 in the isochronal annealing series.

T_{anneal} °C	$Q(0)_{D_2}$ cm^{-1}	$Q(0)_{HD}$ cm^{-1}	$Q(0)_{H_2}$ cm^{-1}	$Q(1)_{H_2}$ cm^{-1}	ω_e cm^{-1}	$\chi_e\omega_e$ cm^{-1}	k eV/Å^2	D_0 eV	α 10^8 cm^{-1}	r_0 Å	Δ_{op}(Calc.) cm^{-1}
300	2996.5	3637.7	4169.3	4161.6	4403	117	36.0	5.1	1.87	0.742	3.9
400	2992.1	3631.5	4161.9	4155.0	4401	120	35.9	5.0	1.89	0.742	4.1
450	2989.6	3628.5	4157.6	4150.5	4398	120	35.8	5.0	1.89	0.743	4.1
500	2989.0	3627.5	4157.1	4149.6	4398	121	35.9	5.0	1.90	0.743	4.1
550	2989.3	3627.7	4157.9	4150.0	4399	122	35.9	4.9	1.91	0.743	4.2
600	2989.6	3628.1	4158.1	4150.7	4400	121	35.9	4.9	1.90	0.743	4.2
$(H_2)_{gas}$					4413	127	36.1	4.8	1.95	0.741	4.5
$(H_2)_{Si}^{plat}$					4406	124	36.0	4.8	1.93	0.742	4.3
$(H_2)_{Si}^{int}$					4015	194	29.9	2.6	2.41	0.788	7.8

2. *Isothermal annealing*

In order to separate the effect of thermal stability of H_2 from the influence of lattice damage an isothermal annealing series was performed.

Figure 4(a) presents Raman spectra taken for a ZnO sample hydrogenated at 1000 °C and subsequently annealed at 300 °C. As the annealing time grows the LVM frequency of the H_2 molecule red-shifts and saturates at about 4155 cm^{-1} after 41 h.

Assuming that the concentration N of the defects affecting the LVMs of H_2 is given by a simple exponential decay,

$$\frac{dN}{dt} = -N\nu = -N\nu_0 \exp\left(-\frac{\Delta E_a}{kT}\right), \quad (5)$$

and the frequency shift is proportional to N we obtain

$$\sigma(t) = (\sigma_0 - \sigma_\infty)\exp\left[-\nu_0 t \exp\left(-\frac{\Delta E_a}{kT}\right)\right] + \sigma_\infty. \quad (6)$$

Here $\nu_0 = 1.17\times10^{13}$ s^{-1} is equal to the TO phonon frequency of ZnO, and ΔE_a is the activation energy of the annealing process.

The solid line in Fig. 4(b) shows the best-fit curve with $\Delta E_a = 2$ eV and a saturated frequency of $\sigma_\infty = 4155$ cm^{-1}. Note that due to the logarithmic dependence of ΔE_a from ν_0 [$\Delta E_a = kT\ln(\nu_0/\nu)$] the activation energy is rather insensitive to the variations of ν_0. For instance, a deviation by two orders of magnitude results only in a 10% change of ΔE_a. The value of σ_∞ still deviates by about 10 cm^{-1} from the vibrational mode of o-H_2 after 1-h anneal at 500 °C. A possible reason for this could be the presence of another defect(s) with different activation energy(ies).

The missing ortho-para splitting of the $Q(1)$ mode (see Fig. 4) may also indicate the presence of another defect(s). In addition to the shift of the LVM its perturbation may also break up the spherical symmetry of the molecular potential and split the $J = 1$ state yielding similar frequencies for $Q(1)$ and Q(0) [40].

C. Temperature dependence of the Raman signals

Figure 5(a) shows temperature-dependent Raman spectra of H_2 obtained for a sample annealed at 450 °C. The local

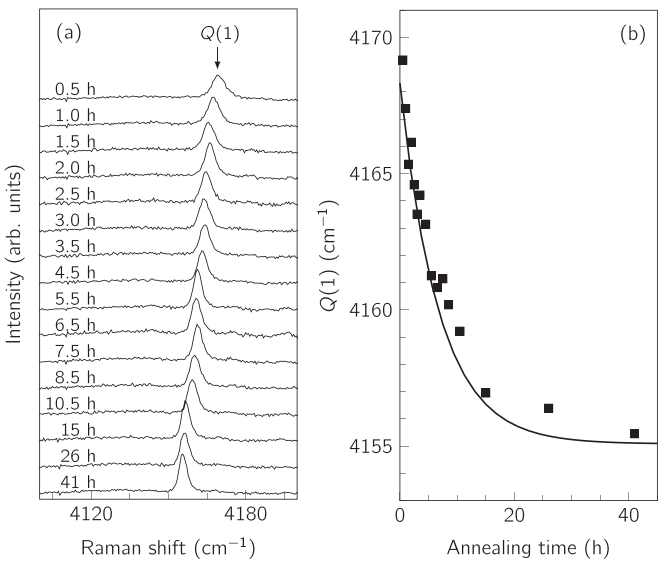

FIG. 4. Isothermal annealing series of H_2 performed at 300 °C. Raman spectra ($T \leqslant 55$ K) of a ZnO sample hydrogenated at 1000 °C (a). LVM frequency of H_2 as a function of annealing time (b).

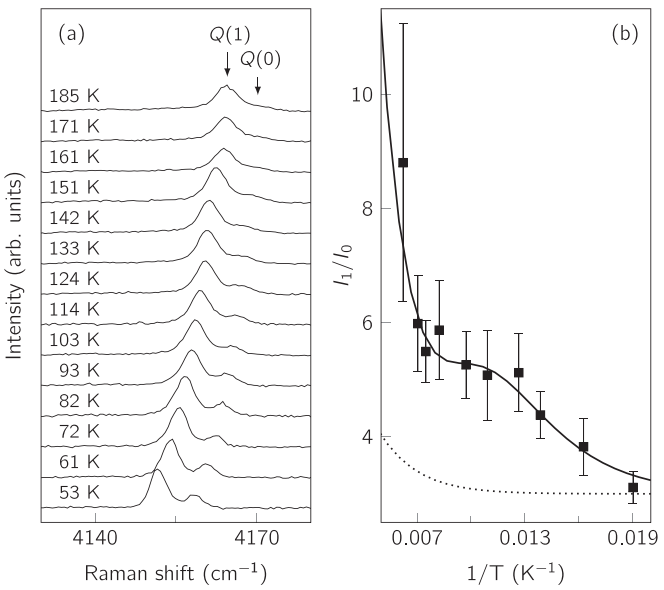

FIG. 5. Temperature-dependent Raman spectra of H_2 (a). Intensity ratio of the $Q(1)$ and $Q(0)$ modes (b). The solid line is a guide for the eye. The dotted line is the I_1/I_0 ratio of gaseous H_2.

temperature in the excitation volume was determined from the intensity ratio of the Stokes to anti-Stokes lines of the lattice phonons. Due to the weak intensity of the anti-Stokes component the lowest temperature that could be determined in this way was 50 K. The $Q(1)$ and $Q(0)$ modes of o- and p-H_2 are clearly seen in the spectra at low temperatures. With increasing temperature the lines blue-shift and broaden. Additionally, the $Q(0)$ mode becomes weaker, whereas the $Q(1)$ mode remains unchanged. The intensity ratio I_1/I_0 of the two modes is presented in Fig. 5(b).

The dotted line in the figure shows the ratio of I_1/I_0 for gaseous H_2, which can be obtained from

$$\frac{I_1}{I_0} = n_{op}\frac{1+\sum_{J=2,4,\ldots}^{\infty} N_{J1}\exp(-E_{J0}/kT)}{1+\sum_{J=3,5,\ldots}^{\infty} N_{J0}\exp(-E_{J1}/kT)}, \qquad (7)$$

where $N_{J1(0)}$ and $E_{J1(0)}$ are the degeneracy ratios of the rotational J to the $J = 1(0)$ states and the energy differences between these states, respectively [41]. The prefactor $n_{op} = 3$ accounts for the degeneracies of the $I = 1$ and $I = 0$ nuclear spin states of o- and p-H_2, respectively. For gaseous H_2 this value does not change due to a negligible ortho-to-para conversion rate.

As the temperature rises, the $J = 2$ rotational state becomes populated at the expense of the $J = 0$ state of p-H_2 resulting in the enhancement of I_1/I_0. The intensity of the $J = 1$ state does not change noticeably in this temperature range due to the larger value of E_{31} (587 cm^{-1}) compared to E_{20} (354 cm^{-1}).

At low temperatures the intensity ratio I_1/I_0 for H_2 in ZnO matches that of the free species. At elevated temperatures, however, it increases faster than in the case of gaseous H_2. This behavior can be explained by either a larger $N_{J1(0)}$ or a smaller $E_{J1(0)}$ for the molecule positioned in the ZnO lattice. We favor the former situation for the following reasons. As depicted in Fig. 6 the value of E_{20} (deduced from Table I) is close to a phonon combination mode at around 320 cm^{-1} and the A_1(TO) mode at 379 cm^{-1}, whereas E_{31} is practically in resonance with the E_1(LO) mode of ZnO at 591 cm^{-1}. The resonance coupling between rotational modes of H_2 and the lattice phonons should strongly enhance the degeneracy factors of H_2 in ZnO resulting in the deviation of the temperature dependencies of H_2 in ZnO compared to those of the gaseous molecule. This situation is not unique and was already reported for interstitial H_2 in Si [42,43].

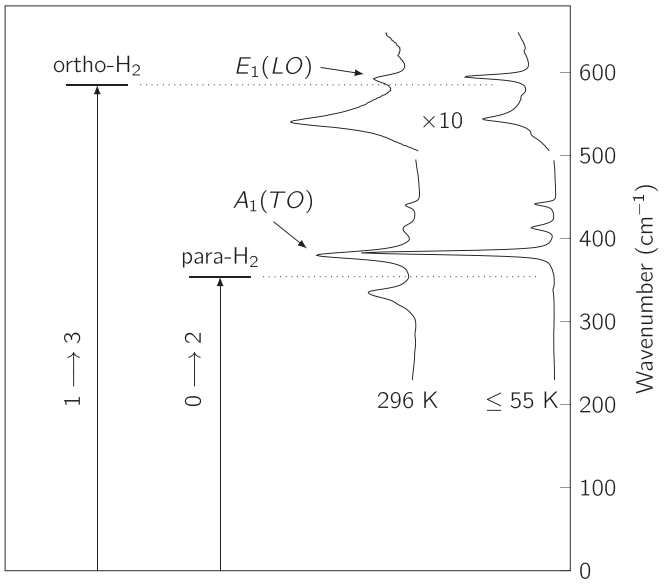

FIG. 6. Resonance between the lattice phonons of ZnO and the rotational states of H_2. Presented are the corresponding Raman spectra in the phonon region at 296 and ⩽55 K.

The value of I_1/I_0 shows a plateau in the temperature range 100–140 K. We explain this behavior by an ortho-to-para conversion which becomes significant on the time scale of the experiment (30 min) while competing with the thermal excitation to the $J = 2$ state of p-H_2 (see Sec. III E). The dependency of the ortho-to-para ratio n_{op} in Eq. (7) on temperature and time prevented us from determining the parameters N_{20} and E_{20}.

The absence of the $Q(2)$ signal in the Raman spectra at elevated temperatures is explained by a line broadening due to the resonance coupling between the rotational states and the lattice phonons, similar to the case of interstitial H_2 in Si [43]. Furthermore, it is expected that the lattice potential lifts the fivefold degeneracy of the $J = 2$ state also contributing to the broadening of the $Q(2)$ transition.

Finally, we note the blue-shift of the LVM with increasing temperature. Of all semiconductor hosts a similar behavior was reported only for H_2 trapped within hydrogen platelets in Si [16], whereas the majority of semiconductors, where the molecule was identified, revealed a red-shift (interstitial sites and voids in Si [5,17,42] and GaAs [44], voids in Ge [45]). Nonmonotonic behavior of the LVM frequencies with the temperature was reported for H_2 trapped in metal-organic frameworks MOF-5 [46–48] and ZIF-8 [49], whereas LVM was found to be independent of temperature for the molecule trapped in C_{60} [50].

D. Polarized Raman spectra

The scattering intensity in Raman measurements is given by

$$I_s = |\boldsymbol{e}_i \cdot \hat{\Re} \cdot \boldsymbol{e}_s|^2, \qquad (8)$$

where $\boldsymbol{e}_i$ and $\boldsymbol{e}_s$ are the polarization vectors of the incident and scattered light, respectively, and $\hat{\Re}$ is the Raman tensor, which is determined by the symmetry of the scattering center.

Polarized Raman spectra presented in Fig. 7 reveal that the intensities of H_2 related LVMs are independent of the crystal orientation and have nonzero intensities only if the polarizations of the incident and scattered light are parallel to each other ($\boldsymbol{e}_i \parallel \boldsymbol{e}_s$). We take this as a strong indication that the molecule in ZnO is a free rotator without any preferential orientation in the crystalline lattice.

The depolarization ratio Δ is defined as the ratio of the scattered light intensity polarized perpendicular to the excitation light to the intensity parallel to $\boldsymbol{e}_i$. For H_2 in ZnO we find that

$$\Delta_{H_2}^{ZnO} = (1.02 \pm 0.80)\times 10^{-2}. \qquad (9)$$

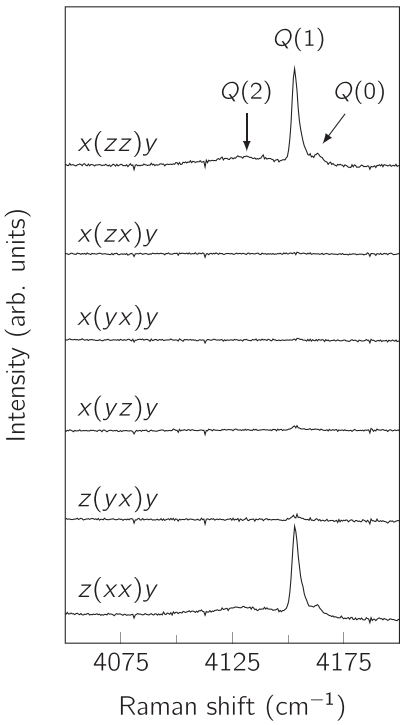

FIG. 7. Polarized Raman spectra of H_2 in ZnO obtained at $T \leqslant 50$ K.

From here the Raman tensor of H_2 in ZnO can be obtained (with z parallel to the interatomic distance) [51]:

$$\hat{\Re} \sim \begin{pmatrix} 1 & 0 & 0 \\ 0 & 1 & 0 \\ 0 & 0 & 1.45 \pm 0.29 \end{pmatrix}, \qquad (10)$$

which within the error bars of our measurements agrees with the values known from the literature for free H_2 [52–54].

E. Ortho-para conversion

Figure 8(a) shows the Raman spectra of H_2 in ZnO obtained for a sample stored and measured at 79 K with an integration time of 30 min. The intensity ratio of the $Q(1)$ and $Q(0)$ modes given in Fig. 8(b) decreases with the storage time. The solid line in the figure is the best-fit curve assuming the exponential ortho-para conversion process,

$$\frac{I_1}{I_0} = (2.3 \pm 0.3)\exp(-t/\tau_{op}) + (2.4 \pm 0.2), \qquad (11)$$

yielding the characteristic conversion time of $\tau_{op} = 7.5 \pm 2.0$ h at 79 K. Note that the starting value of $I_1/I_0|_{t=0} = 4.7$ deviates from the ortho-to-para ratio of 3 due to the partial excitation of the p-H_2 rotational state $J = 0 \rightarrow 2$ state; see Eq. (7).

After the nuclear spin of H_2 reached the thermal equilibrium, the sample was cooled down below 55 K in order to freeze out the ortho-para ratio of 79 K. Figure 9 shows Raman spectra of H_2 recorded at temperatures below 55 K directly after the cooling down and after subsequent annealing of the sample at room temperature. Already the first 30 min bring the I_1/I_0 ratio back to the equilibrium value of 3.1 ± 0.6

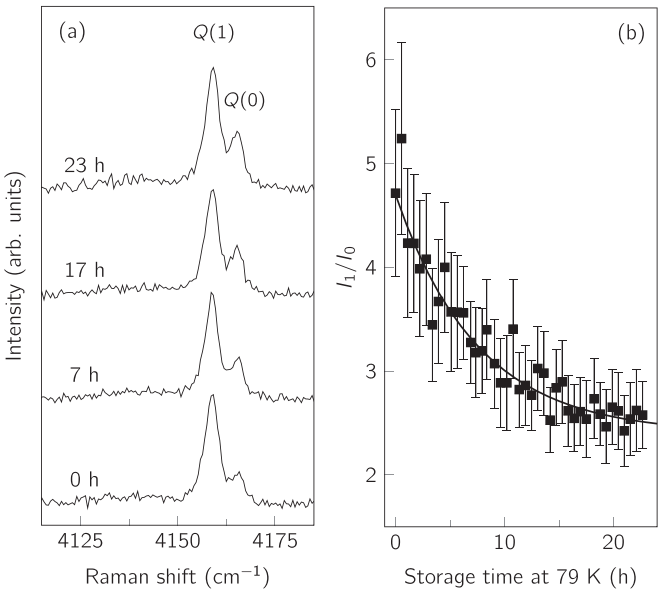

FIG. 8. Ortho-to-para conversion process of H_2 in ZnO at 79 K. Raman spectra taken at 79 K (a). The intensity ratio of the $Q(1)$ and $Q(0)$ vibrational modes as a function of the storage time (b). The solid line shows the best-fit curve (see text).

which does not change after 44 h of room temperature annealing. Based on this we conclude that the para-to-ortho back conversion rate τ_{po} at room temperature is faster than 0.5 h. Since the warm up and cool down time of our Raman setup could not be less than 30 min a precise definition of τ_{po} was not possible.

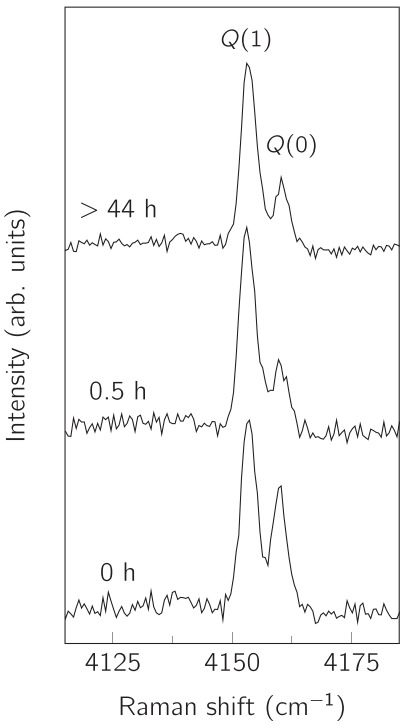

FIG. 9. Para-to-ortho conversion process of H_2 in ZnO at room temperature after annealing at the depicted time. The Raman spectra were recorded at $T \leqslant 55$ K.

TABLE II. LVMs and ortho-para conversion rates of H_2 trapped at different lattice sites in Si and ZnO.

Host	Trap	LVM (cm^{-1})	τ at LN_2 (h)	τ at RT (h)	Ref.
Si	T_d site	3627	229 ± 14	8.1 ± 0.5	[15,38]
	Oxygen	3736	238 ± 43	4.5 ± 0.5	[15,42]
	K complexes	3830	62 ± 15	8 ± 2	[17,56]
	Platelets	4150	9 ± 4	6 ± 4	[16,57]
ZnO	Interstitial	4154	7.5 ± 2.0	$\leqslant 0.5$	This work

The results obtained are summarized in Table II together with the ortho-to-para conversion rates of H_2 trapped at various sites in Si—the only semiconductor host where the ortho-para conversion process of the molecule was investigated. As one can see, the conversion rates decrease with decreasing deviation between the LVMs of H_2 trapped at the defects and the gaseous H_2. This trend indicates a correlation for the coupling between the molecule and the host lattice. Various reasons for the conversion between the molecular species have been discussed in the literature for Si [15]. Here we consider the interaction of the nuclear spin of H_2 with nearby magnetic moments of the host atoms [55].

Of all constituents of ZnO only ^{67}Zn with a natural abundance of $p(^{67}\mathrm{Zn}) = 4.1\%$ exhibits a nonzero magnetic moment. In an assumption that the preferential diffusion path of H_2 is along the c axis [58], the thermally activated motion of the molecule in the c channel could provide the magnetic field gradient necessary for the ortho-para conversion process. The probability that H_2 did not face at least one ^{67}Zn atom after N_δ diffusion steps between the neighboring O interstitial sites is

$$P = [1 - p(^{67}\mathrm{Zn})]^{3(N_\delta+1)}. \quad (12)$$

The number of steps N_δ at which $P = 0.5$ corresponds to the characteristic diffusion length $l = N_\delta\delta$ at which the ortho-to-para conversion takes place. Here, $\delta = 2.60$ Å is the distance between two neighboring O sites [59]. For the ortho-para conversion rate of 7.5 h obtained at 79 K the diffusion constant for H_2 parallel to the c axis accounts 5.1×10^{-19} cm^2/s. Since the prefactor D_0 for interstitial diffusion is about 2×10^{-4} cm^2/s [42,60,61], the estimation of the diffusion barrier E_a yields 0.23 eV. Due to the logarithmic dependence on D_0, the diffusion barrier is only weakly influenced by the uncertainty of the prefactor. With the value of E_a the back conversion at room temperature is expected to happen within a fraction of seconds. Note that the estimated diffusion barrier of H_2 is about half the value of that for the interstitial atomic hydrogen [62].

We emphasize that this is only an estimate. Recently, it was shown that ortho-para conversion of interstitial H_2 in Si cannot be mediated by nearby ^{29}Si [15]. A significantly better signal-to-noise ratio of Raman spectra as well as theoretical analysis are prerequisite to distinguish between different mechanisms of the ortho-para conversion.

F. Position in the lattice

Figure 10 presents depth profiles of H_O and H_2 obtained for a ZnO sample hydrogenated at 1000 °C and subsequently annealed at 400 °C. The spectra were recorded at different excitation spots along the y axis (see Fig. 1). In the near surface region the H_2 related LVMs are broadened due to the lattice imperfections. The anticorrelation of the depth profiles of H_2 and H_O near the surface implies that trapping of hydrogen at the oxygen vacancy is energetically more favorable than a molecule formation. This finding agrees with calculations of formation energies of hydrogen-related defects in ZnO by Du and Biswas [22]. It follows also from the figure that the annealing at 400 °C reduces the formation depth of H_O from 280 (directly after the hydrogenation) to about 200 μm (see Ref. [27]).

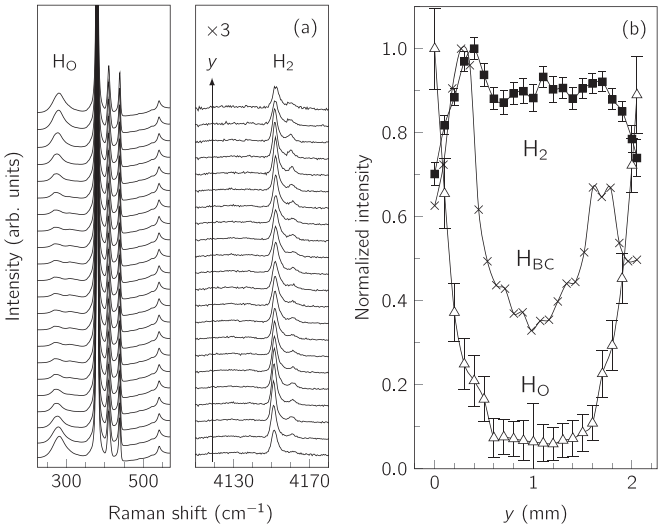

FIG. 10. Depth profiles obtained for a ZnO sample hydrogenated at 1000 °C and subsequently annealed at 400 °C. (a) Raman spectra recorded at $T \leqslant 55$ K as a function of y (see Fig. 1). (b) Normalized intensities of the H_O (triangles) and H_2 (squares) signals. For comparison a depth profile of H_{BC} (×) directly after hydrogenation is included (see Ref. [27]). Here the "y" scale is compressed by a factor of 0.89 for adjustment.

Theory suggests three different positions of the molecule in the ZnO lattice:

(i) Van de Walle [18] and Wardle *et al.* [19] found that the interstitial H_2 is positioned at the antibonding Zn site in the c channel and is roughly aligned along the c axis. No rotational barrier for the molecule was calculated. The interatomic distance as well as the LVM of interstitial H_2 were found to be very close to those of the gaseous H_2 [19]. Moreover, the formation energy for H_2 was found to be practically the same as for two isolated interstitial hydrogen atoms.

(ii) Karazhanov and Ulyashin have found that the only stable hydrogen dimer in unstrained ZnO is a so-called H_2^* complex with one hydrogen atom (H1) bound to oxygen and the second one (H2) to a nearby zinc atom with only a weak coupling between H1 and H2 [20]. The interatomic distance was found to be 1.25 Å. The H_2^* complex dissociates, however, upon charge transfer caused by a lattice strain or an oxygen deficiency into an interstitial and a substitutional hydrogen atom,

$$H_2^* \rightarrow H_i + H_O.$$

(iii) Du and Biswas have determined that the molecule is located in the oxygen vacancy V_O rather than at the interstitial site [22]. The formation process of this complex is given by the reaction,

$$V_O^{2+} + 2H_i^- \rightarrow V_O^{2+}H_2 + 2e^-.$$

The molecule was found to be located preferentially close to the surface near the boundary of the surface depletion region. The dissociation process was suggested to happen via

$$V_O^{2+}H_2 \rightarrow H_i^+ + H_O^+.$$

The results presented in Fig. 10 show the anticorrelation behavior between H_O and H_2 signals which rules out the oxygen vacancy as a trapping center for the molecule. This conclusion is supported by recent calculations of the LVM frequency of H_2 located at the V_O to be 3991 cm^{-1}, which significantly deviates from the experimentally observed value [63]. In addition, the negatively charged interstitial hydrogen H_i^- is unstable for all Fermi levels in the band gap preventing the formation mechanism proposed by Du and Biswas [18,22,64].

The model of H_2^* is also not consistent with our experimental findings on the LVMs: The frequencies, the ortho-para splitting, the temperature behavior of the Q modes, the ortho-para conversion process, and the polarization properties of the Raman signals cannot be explained by the H_2^* model. In addition, IR absorption measurements performed as a part of this investigation have shown no signal for all isotopic combinations of the molecule, which implies that the complex exhibits no dipole moment.

Thus, we conclude that our results are more consistent with a model of H_2 as an almost free rotator only weakly interacting with the host lattice. Room temperature uniaxial stress measurements performed as a part of this study did not reveal any shift or additional splitting of the LVM of H_2 in support of this assignment. This agrees with a model proposed earlier by Van de Walle as well as Wardle *et al.* [18,19]. These authors, however, have found that H_2 is aligned parallel to the c axis. A similar situation was reported for the interstitial molecule in Si with a rotational barrier of at least 0.17 eV [65]. Nevertheless, the experimentally observed behavior of H_2 in Si was consistent with a freely rotating species. Only the $J = 2$ state was split into two components due to the interaction with the host lattice [66]. In the wurzite structure even the $J = 1$ state is supposed to split into two sublevels which belong to a nondegenerated A_1 and a twofold degenerated E representation of the C_{3v} point group. No splitting of the $Q(1)$ mode, however, was observed due to a weak perturbation of the host.

The wurtzite-type crystal structure possesses two highly symmetric interstitial sites: an octahedral O (O_{int}) and a tetrahedral T one. To the best of our knowledge the formation energies for H_2 at these interstitial sites in ZnO have not been considered theoretically. On the other hand, for other wurtzite-type semiconductors it was found that the O site is the most likely location for the molecule [67,68]. A simple estimate of the open space at the two interstitial sites in ZnO reveals for H_2 a larger volume at the O site compared to the T site. Based on this simple consideration and in agreement with theory we tentatively suggest O to be the trapping site for the molecule observed in our experiments.

An interstitial site is not the only position that can provide enough space to trap the molecule. The formation of one-, two- and three-dimensional voids filled with hydrogen during the crystal growth [69] or after proton implantation [70,71] was reported in the literature. Zinc vacancies formed via ion bombardment were found to coalesce into the bubbles filled with hydrogen after annealing at temperatures 200 °C–500 °C [70]. Further treatments at higher temperatures releases the hydrogen from those traps. It was also shown, that subsequent annealing results in a significant decrease of lattice strain [71]. Recently, zinc vacancy-related defects were shown to be formed after annealing ZnO in oxygen or nitrogen atmosphere above 900 °C [72].

The results reported here can be understood in terms of vacancy clustering. H_{BC} is the predominant hydrogen species directly after the hydrogenation at 1000 °C. However, its concentration is only half in the sample center compared to the maximum closer to the surface. Apparently, the presence of other defects, like vacancy clusters, slows down the formation of H_{BC} in the bulk of the sample. The dependence of the LVM frequency of H_2 on temperature of hydrogenation or annealing (see Figs. 3 and 4) could also be related to vacancy agglomeration during the hydrogenation process. Figure 3 indicates that the threshold temperature for the clustering is about 200 °C. Ripening of the vacancy clusters with annealing temperature or time provides bigger volume for the molecules and leads to the red-shift of the LVM frequencies and the line narrowing. An equilibrium state is reached at 500 °C.

The vacancy cluster formation should strongly depend on the treatment temperature, which, in turn, can explain the frequency shift presented in Fig. 2. No hydrogen molecules were observed for the samples hydrogenated below 800 °C further favoring the vacancy clustering model. Moreover, both the threshold temperature for the clustering and the temperature at which the LVM frequency of H_2 stabilizes are in good agreement with the results of positron annihilation experiments on open-volume defects assigned to vacancy clusters in ZnO without hydrogen [73]. Theoretical investigation of H_2 is called for to unambiguously assign the trapping center for the hydrogen molecule.

IV. CONCLUSIONS

In summary, a Raman scattering study of H_2 in ZnO is presented. The molecule was found to be a nearly free rotator stable in the temperature range 300 °C–700 °C. Interstitial hydrogen (H_{BC}) is identified as the major source for the molecule formation. The dissociation happens both via forming substitutional (H_O) and interstitial (H_{BC}) hydrogen. An ortho-para conversion rate at 79 K was found to be 7.5 h, whereas the back conversion at room temperature occurs within less than 0.5 h. A coupling between the rotational states of H_2 and lattice phonons are found to influence the ro-vibrational states of the molecule. The local vibrational modes shift during the annealing procedures which is assigned to the lattice imperfection. The interstitial site or vacancy clusters are suggested as the most likely position for the molecule in the ZnO lattice.

ACKNOWLEDGMENTS

This work was partially funded by the Deutsche Forschungsgemeinschaft (Grant No. LA 1397/4-1). The authors thank M. Nacke for some EBSD characterizations. F. Herklotz is acknowledged for fruitful discussions.

[1] A. Mainwood and A. M. Stoneham, Physica B **116**, 101 (1983).
[2] J. W. Corbett, S. N. Sahu, T. S. Shi, and L. C. Snyder, Phys. Lett. A **93**, 303 (1983).
[3] J. Vetterhöffer, J. Wagner, and J. Weber, Phys. Rev. Lett. **77**, 5409 (1996).
[4] R. E. Pritchard, M. J. Ashwin, J. H. Tucker, R. C. Newman, E. C. Lightowlers, M. J. Binns, S. A. McQuaid, and R. Falster, Phys. Rev. B **56**, 13118 (1997).
[5] A. W. R. Leitch, V. Alex, and J. Weber, Phys. Rev. Lett. **81**, 421 (1998).
[6] M. Hiller, E. Lavrov, and J. Weber, Physica B **376–377**, 142 (2006).
[7] G. A. Shi, M. Saboktakin, M. Stavola, and S. J. Pearton, Appl. Phys. Lett. **85**, 5601 (2004).
[8] E. V. Lavrov, F. Herklotz, and J. Weber, Phys. Rev. Lett. **102**, 185502 (2009).
[9] L. D. Landau and E. M. Lifschitz, *Quantum Mechanics: Non-Relativistic Theory*, 3rd ed. (Pergamon Press, Oxford, 1977).
[10] K. Pachucki and J. Komasa, Phys. Rev. A **77**, 030501 (2008).
[11] B. P. Stoicheff, Can. J. Phys. **35**, 730 (1957).
[12] C. G. Van de Walle, Phys. Rev. Lett. **80**, 2177 (1998).
[13] M. Hiller, E. V. Lavrov, and J. Weber, Phys. Rev. Lett. **98**, 055504 (2007).
[14] M. Hiller, E. V. Lavrov, and J. Weber, Phys. Rev. Lett. **99**, 209901(E) (2007).
[15] C. Peng, M. Stavola, W. B. Fowler, and M. Lockwood, Phys. Rev. B **80**, 125207 (2009).
[16] M. Hiller, E. V. Lavrov, and J. Weber, Phys. Rev. B **80**, 045306 (2009).
[17] S. Socher, E. V. Lavrov, and J. Weber, Phys. Rev. B **86**, 125205 (2012).
[18] C. G. Van de Walle, Phys. Rev. Lett. **85**, 1012 (2000).
[19] M. G. Wardle, J. P. Goss, and P. R. Briddon, Phys. Rev. B **72**, 155108 (2005).
[20] S. Z. Karazhanov and A. G. Ulyashin, Phys. Rev. B **78**, 085213 (2008).
[21] S. Z. Karazhanov, Phys. Status Solidi B **247**, 950 (2010).
[22] M.-H. Du and K. Biswas, Phys. Rev. Lett. **106**, 115502 (2011).
[23] G. Müller and R. Helbig, J. Phys. Chem. Solids **32**, 1971 (1971).
[24] R. Helbig, J. Cryst. Growth **15**, 25 (1972).
[25] T. C. Damen, S. P. S. Porto, and B. Tell, Phys. Rev. **142**, 570 (1966).
[26] E. V. Lavrov, F. Herklotz, and J. Weber, Phys. Rev. B **79**, 165210 (2009).
[27] S. G. Koch, E. V. Lavrov, and J. Weber, Phys. Rev. B **89**, 235203 (2014).
[28] D. G. Thomas and J. J. Lander, J. Chem. Phys. **25**, 1136 (1956).
[29] B. B. Varga, Phys. Rev. **137**, A1896 (1965).
[30] B. H. Bairamov, A. Heinrich, G. Irmer, V. V. Toporov, and E. Ziegler, Phys. Status Solidi B **119**, 227 (1983).
[31] A. Bikowski and K. Ellmer, J. Appl. Phys. **113**, 053710 (2013).
[32] G. A. Shi, M. Stavola, S. J. Pearton, M. Thieme, E. V. Lavrov, and J. Weber, Phys. Rev. B **72**, 195211 (2005).
[33] F. Herklotz, E. V. Lavrov, Vl. Kolkovsky, J. Weber, and M. Stavola, Phys. Rev. B **82**, 115206 (2010).
[34] M. D. McCluskey, S. J. Jokela, K. K. Zhuravlev, P. J. Simpson, and K. G. Lynn, Appl. Phys. Lett. **81**, 3807 (2002).
[35] P. M. Morse, Phys. Rev. **34**, 57 (1929).
[36] C. L. Pekeris, Phys. Rev. **45**, 98 (1934).
[37] E. E. Chen, M. Stavola, W. B. Fowler, and P. Walters, Phys. Rev. Lett. **88**, 105507 (2002).
[38] E. V. Lavrov and J. Weber, Phys. Rev. Lett. **89**, 215501 (2002).
[39] M. Hiller, E. V. Lavrov, and J. Weber, Phys. Rev. B **71**, 045208 (2005).
[40] D. White and E. N. Lassettre, J. Chem. Phys. **32**, 72 (1960).
[41] L. D. Landau and E. M. Lifschitz, *Statistical Physics*, Part 1, 3rd ed. (Pergamon Press, Oxford, 1980).
[42] M. Hiller, E. V. Lavrov, and J. Weber, Phys. Rev. B **74**, 235214 (2006).
[43] S. Koch, E. V. Lavrov, and J. Weber, Phys. Rev. B **83**, 233203 (2011).
[44] E. Lavrov and J. Weber, Physica B **340–342**, 329 (2003).
[45] M. Hiller, Diploma thesis (unpublished).
[46] S. Bordiga, J. G. Vitillo, G. Ricchiardi, L. Regli, D. Cocina, A. Zecchina, B. Arstad, M. Bjorgen, J. Hafizovic, and K. P. Lillerud, J. Phys. Chem. B **109**, 18237 (2005).
[47] S. A. FitzGerald, K. Allen, P. Landerman, J. Hopkins, J. Matters, R. Myers, and J. L. C. Rowsell, Phys. Rev. B **77**, 224301 (2008).
[48] J. G. Vitillo, L. Regli, S. Chavan, G. Ricchiardi, G. Spoto, P. D. C. Dietzel, S. Bordiga, and A. Zecchina, J. Am. Chem. Soc. **130**, 8386 (2008).
[49] S. N. Yurchenko, B. Assfour, E. V. Lavrov, and G. Seifert, RSC Adv. **2**, 9839 (2012).
[50] M. Ge, U. Nagel, D. Hüvonen, T. Rõõm, S. Mamone, M. H. Levitt, M. Carravetta, Y. Murata, K. Komatsu, J. Y.-C. Chen, and N. J. Turro, J. Chem. Phys. **134**, 054507 (2011).
[51] E. B. Wilson, J. C. Decius, and P. C. Cross, *Molecular Vibrations* (Dover, New York, 1980).
[52] D. M. Bishop and J. Pipin, Int. J. Quantum Chem. **45**, 349 (1993).
[53] U. Hohm, Chem. Phys. **179**, 533 (1994).
[54] X. Li, C. Ahuja, J. F. Harrison, and K. L. C. Hunt, J. Chem. Phys. **126**, 214302 (2007).
[55] E. Wigner, Z. Phys. Chem. Abt. B **23**, 28 (1933).
[56] K. Murakami, K. Ishioka, M. Kitajima, S. Tateishi, K. Nakanoya, T. Mori, and S. Hishita, Physica B **273–274**, 188 (1999).
[57] N. Fukata, S. Sasaki, K. Murakami, K. Ishioka, K. G. Nakamura, M. Kitajima, S. Fujimura, J. Kikuchi, and H. Haneda, Phys. Rev. B **56**, 6642 (1997).
[58] M. G. Wardle, J. P. Goss, and P. R. Briddon, Phys. Rev. Lett. **96**, 205504 (2006).

[59] O. Madelung, ed., *Semiconductors: Data Handbook* (Springer-Verlag, Berlin/Heidelberg/New York, 2004).
[60] E. V. Lavrov, J. Weber, and F. Börrnert, Phys. Rev. B **77**, 155209 (2008).
[61] V. P. Markevich and M. Suezawa, J. Appl. Phys. **83**, 2988 (1998).
[62] F. Börrnert, E. V. Lavrov, and J. Weber, Phys. Rev. B **75**, 205202 (2007).
[63] J. Koßmann and C. Hättig, Phys. Chem. Chem. Phys. **14**, 16392 (2012).
[64] A. Janotti and C. G. Van de Walle, Nat. Mater. **6**, 44 (2007).
[65] B. Hourahine, R. Jones, S. Öberg, R. C. Newman, P. R. Briddon, and E. Roduner, Phys. Rev. B **57**, R12666 (1998).
[66] G. A. Shi, M. Stavola, W. B. Fowler, and E. E. Chen, Phys. Rev. B **72**, 085207 (2005).
[67] S. Limpijumnong and C. G. Van de Walle, Phys. Rev. B **68**, 235203 (2003).
[68] T. Eberlein, L. Huggett, R. Jones, and P. Briddon, Physica B **340–342**, 171 (2003).
[69] P. Skupiński, K. Grasza, A. Mycielski, W. Paszkowicz, E. Łusakowska, E. Tymicki, R. Jakieła, and B. Witkowski, Phys. Status Solidi B **247**, 1457 (2010).
[70] Z. Q. Chen, A. Kawasuso, Y. Xu, H. Naramoto, X. L. Yuan, T. Sekiguchi, R. Suzuki, and T. Ohdaira, Phys. Rev. B **71**, 115213 (2005).
[71] K. S. Chan, L. Vines, K. M. Johansen, E. V. Monakhov, J. D. Ye, P. Parkinson, C. Jagadish, B. G. Svensson, and J. Wong-Leung, J. Appl. Phys. **114**, 083111 (2013).
[72] M. Jiang, D. D. Wang, B. Zou, Z. Q. Chen, A. Kawasuso, and T. Sekiguchi, Phys. Status Solidi A **209**, 2126 (2012).
[73] F. A. Selim, M. H. Weber, D. Solodovnikov, and K. G. Lynn, Phys. Rev. Lett. **99**, 085502 (2007).